Diffraction of gratings with rough edges

Francisco Jose Torcal-Milla[*], Luis Miguel Sanchez-Brea, Eusebio Bernabeu

Applied Optics Complutense Group, Optics Department,
Universidad Complutense de Madrid
Facultad de Ciencias Físicas, Ciudad Universitaria s.n., 28040, Madrid (Spain)
ftorcalmilla@fis.ucm.es

Abstract: We analyze the far field and near field diffraction pattern produced by an amplitude grating whose strips present rough edges. Due to the stochastic nature of the edges a statistical approach is performed. The grating with rough edges is not purely periodic, although it still divides the incident beam in diffracted orders. The intensity of each diffraction order is modified by the statistical properties of the irregular edges and it strongly decreases when roughness increases except for the zero-th diffraction order. This decreasing firstly affects to the higher orders. Then, it is possible to obtain an amplitude binary grating with only diffraction orders -1, 0 and +1. On the other hand, numerical simulations based on Rayleigh-Sommerfeld approach have been used for the case of near field. They show that the edges of the self-images are smoother than the edges of the grating. Finally, we fabricate gratings with rough edges and an experimental verification of the results is performed.

©2008 Optical Society of America

OCIS codes: (050.0050) Diffraction and gratings; (050.2770) Gratings; (030.0030) Coherence and statistical optics; (030.5770) Roughness.

References and links

1. M. Born, and E. Wolf, *Principles of Optics* (Pergamon Press, Oxford, 1980).
2. J. W. Goodman, *Introduction to Fourier Optics* (McGraw-Hill, New York, 1968).
3. E. G. Loewen and E. Popov, *Diffraction gratings and applications* (Marcel Dekker, New York, 1997).
4. M. J. Lockyear, A. P. Hibbins, K. R. White, and J. R. Sambles, "One-way diffraction grating," Phys. Rev. E **74**, 056611 (2006).
5. S. Wise, V. Quetschke, A. J. Deshpande, G. Mueller, D. H. Reitze, D. B. Tanner, and B. F. Whiting, "Phase effect in the diffraction of light: beyond the grating equation," Phys. Rev. Lett. **95**, 013901 (2005).
6. C. Palmer, *Diffraction Grating Handbook* (Richardson Grating Laboratory, New York, 2000).
7. R. Petit, *Electromagnetic Theory of Gratings* (Springer-Verlag, Berlin, 1980).
8. F. Gori, "Measuring Stokes parameters by means of a polarization grating," Opt. Lett. **24**, 584-586 (1999).
9. C. G. Someda, "Far field of polarization gratings," Opt. Lett. **24**, 1657-1659 (1999).
10. G. Piquero, R. Borghi, A. Mondello, and M. Santarsiero, "Far field of beams generated by quasi-homogeneous sources passing through polarization gratings," Opt. Commun. **195**, 339-350 (2001)
11. F. J. Torcal-Milla, L. M. Sanchez-Brea, and E. Bernabeu, "Talbot effect with rough reflection gratings," Appl. Opt. **46**, 3668- 3673 (2007)
12. L.M. Sanchez-Brea, F. J. Torcal-Milla, and E. Bernabeu, "Talbot effect in metallic gratings under Gaussian illumination," Opt. Commun. **278**, 23–27 (2007).
13. L. M. Sanchez-Brea, F. J. Torcal-Milla, and E. Bernabeu, "Far field of gratings with rough strips," J. Opt. Soc. Am. A **25**, 828-833 (2008).
14. W. H. F. Talbot, "Facts relating to optical science," Philos. Mag. **9**, 401–407 (1836).
15. K. Patorski, "The self-imaging phenomenon and its applications," Prog. Opt. **27**, 1–108 (1989).
16. N. Guérineau, B. Harchaoui, and J. Primot, "Talbot effect re-examined: demonstration of an achromatic and continuous self-imaging regime," Opt. Commun. **180**, 199-203 (2000).
17. Y. Lu, C. Zhou, and H. Luo, "Talbot effect of a grating with different kind of flaws," J. Opt. Soc. Am. A **22**, 2662-2667 (2005)
18. P. P. Naulleau and G. M. Gallatin, "Line-edge roughness transfer function and its application to determining mask effects in EUV resist characterization," Appl. Opt. **42**, 3390-3397 (2003).
19. T. R. Michel, "Resonant light scattering from weakly rough random surfaces and imperfect gratings," J. Opt. Soc. Am. A **11**, 1874-1885 (1994).

20. V. A. Doroshenko, "Singular integral equations in the problem of wave diffraction by a grating of imperfect flat irregular strips," Telecommunications and Radio Engineering **57**, 65-72 (2002)
21. M. V. Glazov., and S. N. Rashkeev, "Light scattering from rough surfaces with superimposed periodic structures," Appl. Phys. B **66**, 217–223 (1998)
22. F. Shen and A. Wang, "Fast-Fourier-transform based numerical integration method for the Rayleigh–Sommerfeld diffraction formula," Appl. Opt. **45**, 1102-1110 (2006)
23. P. Beckmann and A. Spizzichino, *The Scattering of Electromagnetic Waves from Rough Surfaces* (Artech House Norwood, 1987).

1. Introduction

Diffraction gratings are one of the most important optical components. It can be defined as an element which produces a periodical modulation in the properties of the incident light beam. Its behaviour in the near and far field is well known [1-7]. Amplitude or phase gratings are used in most applications. Also, other kind of gratings is possible, such as polarization gratings [8-10] or gratings with random microscopic irregularities in the topography [11-13]. In the far field the beam is divided into diffraction orders whose directions are given by the well-known grating equation [1]. The intensity of the diffraction orders is obtained as the square of the Fourier coefficients of the grating [2]. In the near field, Talbot effect is produced when the grating is illuminated with a plane wave [14, 15]. Self-images of the grating are formed at Talbot distances given by $z_T = \lambda / \left\{ 1 - [1 - (\lambda / p)^2]^{1/2} \right\}$ where λ is the wavelength of the incident wave and p is the period of the grating. When the period of the grating is much larger than the wavelength then the Talbot distance simplifies to $z_T = 2p^2 / \lambda$ [16].

Theoretical approaches normally assume that the diffraction gratings present an ideal optical behaviour. However, this assumption is not always right. Flaws or defects can be produced, such as lost strips, during the fabrication process [17-21]. Other non-ideal behaviour is owing to roughness on the surface of the gratings, as it happens for steel tape gratings. Roughness produces a decreasing of the contrast of the self-images [11, 12]. Also, stochastical irregularities in the shape of the edges can be produced. This effect is not normally present in chrome on glass gratings or phase glass gratings, but strips with rough edges can be detected in some other manufacturing processes, such as laser ablation or chemical attack [13, 18].

In this work we theoretically, numerically and experimentally analyze the behaviour of amplitude gratings with rough edges. In particular, the far field intensity distribution and the Talbot effect are studied in detail. Talbot effect is a very important point which must be taken into account in devices that include a diffraction grating which works in near field approach. Rough edges effect can be very important in self-imaging phenomenon, then we will analyse it in detail. In addition, due to the stochastic properties of the edges, a statistical approach needs to be used. We theoretically show that the intensity of the diffraction orders depends on roughness parameters of the edges. Selecting the roughness level for the edges, we can suppress ±3 and higher orders, maintain orders 0 and reduce only slightly orders ±1.

For the near field, a theoretical analysis is not possible since the integrals cannot be solved analytically. Then, a numerical analysis based on Rayleigh-Sommerfeld formalism is performed for determining the properties of the self-images produced by the grating with rough edges [22]. The properties of the self-images are obtained for single realizations and also for statistical averages. In both cases, the edges of the self-images are smoother than the edges of the grating. Finally, we fabricate gratings with rough edges and we analyze the near field behaviour, which is in accordance to the theoretical results.

2. Far field approach

Let us consider an amplitude grating with period p. When the grating presents an ideal optical behaviour, the transmittance can be defined as a Fourier series

$t_p(\xi) = \sum_n a_n \exp(iqn\xi)$, where $q = 2\pi/p$ and a_n are the Fourier coefficients of the grating with n integer. We assume that the edges of the strips are not straight, but present a certain random shape. Therefore, the grating cannot be described as its Fourier series expansion since it is not purely periodic, but as a sum of strips. To mathematically characterize the grating, let us assume that the left and right edges of a single strip are described as $\eta = f_n(\xi)$ and $\eta = g_n(\xi)$, where (ξ, η) are the transversal coordinates at the grating plane and $n = \ldots -2, -1, 0, 1, 2 \ldots$. These functions are not analytical functions, but stochastic with the same statistical parameters. The exact shape of the edges $f_n(\xi)$ and $g_n(\xi)$ is not known but it is possible to describe these functions by means of some stochastic parameters, such as their correlation length T and their standard deviation σ [23]. Let us assume that $f_n(\xi)$ and $g_n(\xi)$ present the same statistical distribution, that $f_n(\xi)$ and $g_n(\xi)$ are totally uncorrelated, and $f_n(\xi)$ and $f_{n'}(\xi')$ are also totally uncorrelated except for $n = n'$. To describe the edges, a normal distribution with standard deviation σ is assumed. We will also assume a Gaussian autocorrelation coefficient with correlation length T. The two-dimensional transmittance of the grating $t(\xi, \eta)$ results

$$t(\xi, \eta) = \sum_{n=-\infty}^{\infty} \Pi(f_n(\xi), g_n(\xi)), \tag{1}$$

being $\Pi(f_n(\xi), g_n(\xi)) = \begin{cases} 1 & f_n(\xi) < \eta < g_n(\xi) \\ 0 & g_n(\xi) < \eta < f_{n+1}(\xi) \end{cases}$.

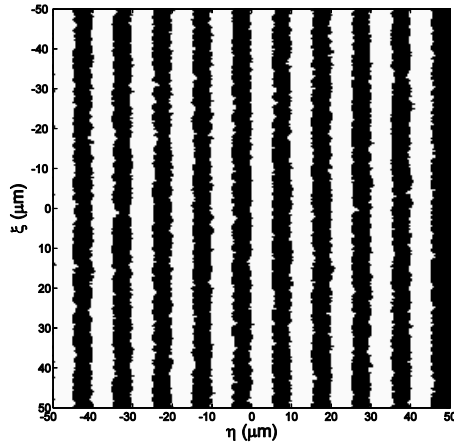An example of the grating proposed is shown in Fig. 1.

Fig. 1. Example of the grating analyzed in this work.

Light passes through the grating and then propagates a distance z. To determine the far field diffraction pattern, Fraunhoffer approach is used

$$U(x, y) = \frac{e^{ik\left(z + \frac{x^2 + y^2}{2z}\right)}}{i\lambda z} \int t(\xi, \eta) U_i(\xi, \eta) e^{-i\frac{k}{z}(x\xi + y\eta)} \, d\xi d\eta, \tag{2}$$

being λ the wavelength of the incident light, $k = 2\pi/\lambda$, x and y the transversal coordinates at the observation plane, z the propagation direction, and $U_i(\xi,\eta)$ the incident field that, for simplicity, we will consider that it is a monochromatic plane wave in normal incidence, $U_i(\xi,\eta) = U_0$. The transmission function only affects to the integration limits into eq. (2). Then, the integral is converted into a summatory of finite integrals. Every one of these integrals corresponds to the contribution to the intensity of every strip of the grating, which has rough edges. Besides, we have truncated the summatory which appears in $t(\xi,\eta)$ to be able to give a clearer equation for the intensity pattern. Thus, the intensity results in

$$I(x,y) = |U(x,y)|^2 = \frac{|U_0|^2}{(\lambda z)^2} \sum_{n,n'=-N/2}^{N/2} \int_{-L/2}^{L/2} d\xi \int_{-L/2}^{L/2} d\xi'$$

$$\int_{g_n(\xi)+(4n+1)p/4}^{f_n(\xi)+(4n-1)p/4} d\eta \int_{g_{n'}(\xi')+(4n'+1)p/4}^{f_{n'}(\xi')+(4n'-1)p/4} e^{-i\frac{k}{z}[x(\xi'-\xi)+y(\eta'-\eta)]} d\eta' \tag{3}$$

where N is the number of strips and L is their length. Performing the integrals in η and η' the intensity results

$$I(x,y) = \frac{|U_0|^2}{(2\pi z\theta_y)^2} \sum_{n,n'} \int_{-L/2}^{L/2} d\xi \int_{-L/2}^{L/2} d\xi' e^{ik\theta_x(\xi-\xi')}$$

$$\left\{ \begin{array}{l} e^{ik\theta_y p(n-n')} e^{ik\theta_y[f_n(\xi)-f_{n'}(\xi')]} + e^{ik\theta_y p(n-n')} e^{ik\theta_y[g_n(\xi)-g_{n'}(\xi')]} \\ -e^{ik\theta_y\frac{p}{2}[2(n-n')+1]} e^{ik\theta_y[f_n(\xi)-g_{n'}(\xi')]} - e^{ik\theta_y\frac{p}{2}[2(n-n')-1]} e^{ik\theta_y[g_n(\xi)-f_{n'}(\xi')]} \end{array} \right\}, \tag{4}$$

where $\theta_x = x/z$ and $\theta_y = y/z$. Assuming the stochastical description of the functions $f_n(\xi)$ and $g_n(\xi)$ given before, the characteristic functions for this distribution result in [23]

$$\left\langle e^{i\alpha f_n(\xi)} \right\rangle = \left\langle e^{i\alpha g_n(\xi)} \right\rangle = e^{-\frac{(\alpha\sigma)^2}{2}},$$

$$\left\langle e^{i\alpha[f_n(\xi)-g_{n'}(\xi')]} \right\rangle = e^{-(\alpha\sigma)^2},$$

$$\left\langle e^{i\alpha[f_n(\xi)-f_n(\xi')]} \right\rangle = \left\langle e^{i\alpha[g_n(\xi)-g_n(\xi')]} \right\rangle = e^{-(\alpha\sigma)^2} \sum_{m=0}^{\infty} \frac{(\alpha\sigma)^{2m}}{m!} e^{-\frac{m(\xi-\xi')^2}{T^2}}, \tag{5}$$

$$\left\langle e^{i\alpha[f_n(\xi)-f_{n'}(\xi')]} \right\rangle = \left\langle e^{i\alpha[g_n(\xi)-g_{n'}(\xi')]} \right\rangle = e^{-(\alpha\sigma)^2}, \quad (n \neq n').$$

being in our case $\alpha = k\theta_y$. Performing an averaging process in (4), using the relationships given in (5), and reorganizing the terms, then the average intensity is

$$\langle I(x,y)\rangle = \frac{2|U_0|^2}{(2\pi z\theta_y)^2}\left\{\left[1-\cos\left(k\theta_y\frac{p}{2}\right)\right]e^{-(k\theta_y\sigma)^2}\sum_{n,n'}e^{ik\theta_y p(n-n')}\int\limits_{-L/2}^{L/2}\int\limits_{-L/2}^{L/2}e^{ik\theta_x(\xi-\xi')}\mathrm{d}\xi\mathrm{d}\xi'\right.$$

$$-Ne^{-(k\theta_y\sigma)^2}\int\limits_{-L/2}^{L/2}\int\limits_{-L/2}^{L/2}e^{ik\theta_x(\xi-\xi')}\mathrm{d}\xi\mathrm{d}\xi' \tag{6}$$

$$\left.+Ne^{-(k\theta_y\sigma)^2}\sum_{m=0}^{\infty}\frac{(k\theta_y\sigma)^2}{m!}\int\limits_{-L/2}^{L/2}\int\limits_{-L/2}^{L/2}e^{ik\theta_x(\xi-\xi')}e^{-\frac{m(\xi-\xi')^2}{T^2}}\mathrm{d}\xi\mathrm{d}\xi'\right\},$$

where the averaging in the intensity is performed on a supposed ensemble of realizations which are obtained, for example, when the grating is moved in the direction parallel to the y axis. Let us assume that the length of the strips L is large, although not infinite. Then, the integrals have a simple analytical solution and the average intensity results

$$\langle I(x,y)\rangle = \frac{|U_0|^2 L^2 p^2 (N+1)^2}{(2\lambda z)^2}e^{-(k\theta_y\sigma)^2}\operatorname{sinc}^2\left(k\theta_y\frac{p}{4}\right)\operatorname{sinc}^2\left(k\theta_x\frac{L}{2}\right)$$

$$\sum_j\operatorname{sinc}^2\left[\pi\frac{p}{\lambda}(N+1)\left(\theta_y-j\frac{\lambda}{p}\right)\right] \tag{7}$$

$$+\frac{2|U_0|^2 NLT\sqrt{\pi}\sigma^2}{(\lambda z)^2}e^{-(k\theta_y\sigma)^2}\sum_{m=1}^{\infty}\frac{(k\theta_y\sigma)^{2(m-1)}}{m!m}e^{-\frac{(kT\theta_x)^2}{4m}}.$$

Comparing this average intensity with that of an amplitude grating without roughness, $\sigma=0$,

$$I(x,y)=\frac{|U_0|^2 L^2 p^2 (N+1)^2}{(2\lambda z)^2}\operatorname{sinc}^2\left(k\theta_y\frac{p}{4}\right)\operatorname{sinc}^2\left(k\theta_x\frac{L}{2}\right)\sum_j\operatorname{sinc}^2\left[\pi\frac{p}{\lambda}(N+1)\left(\theta_y-j\frac{\lambda}{p}\right)\right], \tag{8}$$

we can normalize the Eq. (7) with respect to the maximum intensity of eq. (8), $I_0=\left[|U_0|Lp(N+1)/(2\lambda z)\right]^2$. Also, since N is normally very high, the sinc functions are very narrow and have significant values only when their argument, $\theta_y-j\lambda/p$, is nearly zero. Then the mean intensity results

$$\overline{\langle I(x,y)\rangle}=\operatorname{sinc}^2\left(k\theta_x\frac{L}{2}\right)\sum_j|a_j|^2\,e^{-\left(j\frac{2\pi\sigma}{p}\right)^2}\operatorname{sinc}^2\left[\pi\frac{p}{\lambda}(N+1)\left(\theta_y-j\frac{\lambda}{p}\right)\right]$$

$$+\frac{8\sqrt{\pi}T\sigma^2}{NLp^2}e^{-(k\theta_y\sigma)^2}\sum_{m=1}^{\infty}\frac{(k\theta_y\sigma)^{2(m-1)}}{m!m}e^{-\frac{(kT\theta_x)^2}{4m}}. \tag{9}$$

where $\overline{\langle I(x,y)\rangle}=\langle I(x,y)\rangle/I_0$ is the normalized average intensity and $a_j=\operatorname{sinc}(j\pi/2)$. The first term of (9) corresponds to the diffraction pattern of an amplitude grating but multiplied by a factor which diminishes the intensity of the diffraction orders according to

$$a_j^{rough}=a_j^{perfect}\exp\left[-\left(j2\pi\sigma/p\right)^2/2\right]. \tag{10}$$

In Table 1, the Fourier coefficients for the first five diffraction orders is shown for several values of σ/p.

Table 1. Coefficients a_j^{rough} for the first five diffraction orders of a grating, measured as $a_j \; \exp[-\left(j2\pi\sigma / p\right)^2 / 2]$, for several values of σ / p defined according to (10).

σ / p	j=0	±1	±3	±5
0.0	0.5	0.3183	-0.1061	0.0637
0.1	0.5	0.2613	-0.0180	0.0005
0.2	0.5	0.1445	-0.0001	0.0000

On the other hand, the second term of Eq. (9) is produced only by the roughness of the edges, which affects in both directions, x and y. Roughness produces a Gaussian halo centred in the zero-th order. The width of the halo depends on T along the x direction and σ along the y direction. In Fig. 2, the far field diffraction pattern along the y-axis for different values of T and σ is shown. As it can be seen, when roughness increases, high diffraction orders disappear and the halo grows around the zero-th order. The width of the halo in the y-axis depends on σ. For higher values of σ, the width of the halo diminishes.

Let us analyze two important cases, such as high roughness and low roughness limits. The high roughness limit occurs when $\sigma >> \lambda$. The characteristic functions in (5) are still valid, except the autocorrelation function which is now [23]

$$\left\langle e^{i\alpha[f_n(\xi)-f_n(\xi')]} \right\rangle = \left\langle e^{i\alpha[g_n(\xi)-g_n(\xi')]} \right\rangle = \exp\left[-\left(\xi-\xi'\right)^2 / T_F^2\right], \tag{11}$$

where $T_F = kT / \sigma$. With this substitution and performing the integrals, average intensity results

$$\overline{\left\langle I(x,y)\right\rangle} = \mathrm{sinc}^2\left(k\theta_x \frac{L}{2}\right)\sum_j a_j^2 \; e^{-\left(j\frac{2\pi\sigma}{p}\right)^2} \mathrm{sinc}^2\left[\pi \frac{p}{\lambda}(N+1)\left(\theta_y - j\frac{\lambda}{p}\right)\right]$$
$$+ \frac{8T_F \sqrt{\pi}\sigma^2}{NLp^2} e^{-k^2\left[(\theta_y\sigma)^2+(\theta_x T_F/2)^2\right]}. \tag{12}$$

It is a more simplified result than Eq. (9), since the sum over j disappears.

On the other hand, the slight roughness limit occurs when $\sigma << \lambda$. In this case, Eq. (5) is valid, except the autocorrelation function

$$\left\langle e^{i\alpha[f_n(\xi)-f_n(\xi')]} \right\rangle = \left\langle e^{i\alpha[g_n(\xi)-g_n(\xi')]} \right\rangle = \exp\left[-\left(k\theta_y\sigma\right)^2\right]. \tag{12}$$

Then, the average intensity results

$$\overline{\left\langle I(x,y)\right\rangle} = \mathrm{sinc}^2\left(k\theta_x \frac{L}{2}\right)\sum_j a_j^2 \; e^{-\left(j\frac{2\pi\sigma}{p}\right)^2} \mathrm{sinc}^2\left[\pi \frac{p}{\lambda}(N+1)\left(\theta_y - j\frac{\lambda}{p}\right)\right]. \tag{12}$$

Under this approach the halo disappears and the far field diffraction pattern is equivalent to that of a perfect grating with modified Fourier coefficients.
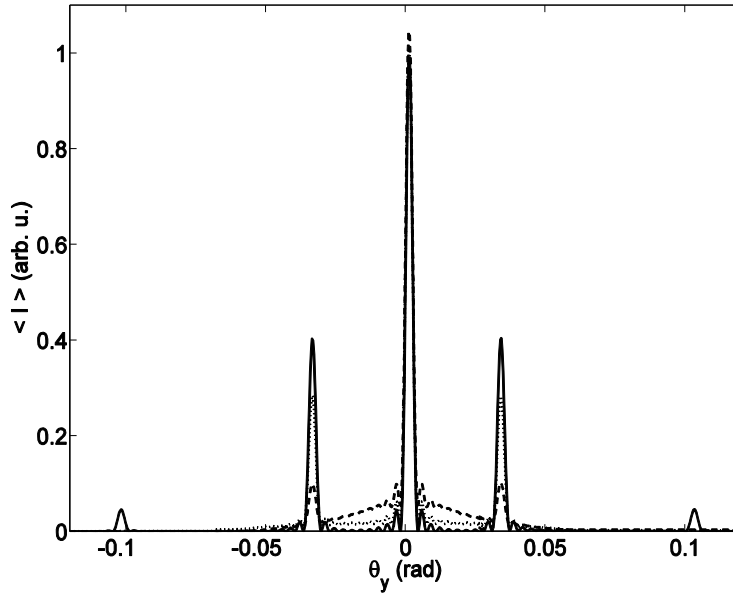
Fig. 2. Diffraction orders intensity for different values of the roughness parameters, when $p = 20$ μm , $\lambda = 0.68$ μm , $T = 50$ μm and $L = 50$ μm : $\sigma \to 0$ (solid line), b) $\sigma = 0.2$ μm (dot line), c), $\sigma = 0.4$ μm (dash line). The order 3 disappears for $\sigma = 0.2$ μm and $\sigma = 0.4$ μm .

3. Self-imaging process in the near field

The intensity distribution in the near field can be obtained in a simple way replacing the Fraunhofer kernel with the Fresnel kernel in (3). Unfortunately it is not possible to obtain analytical solutions for these integrals. As a consequence, we have performed a numerical analysis to determine the characteristics of the intensity distribution in the near field. For the numerical implementation we have used a fast-Fourier-transform based direct integration method which uses the Rayleigh-Sommerfeld approach [22].

In first place we are interested in how the self-images of this grating with rough edges are formed. In Fig. 3 we show for comparison the self-images produced by a perfect grating, that is, without rough edges and in Fig. 4 and Fig. 5, two examples of gratings with rough edges and the first three self-images for different values of σ / p . Although the edges of the grating present a high roughness, the edges of the self-images are quite smooth. The reason is that Talbot effect is a cooperative effect since the intensity at a given point (x, y) of the image is obtained as an integration of the amplitude at the diffraction grating. It performs an averaging in the intensity distribution. In addition, an interferential process happens and produces a kind of speckle in the fringes. For the simulation we have considered a grating with size $150 \mu m \times 300 \mu m$. Since the algorithm does not consider that the grating is periodic, an edge effect is produced. We show the central region of the intensity pattern to avoid this edge effect.
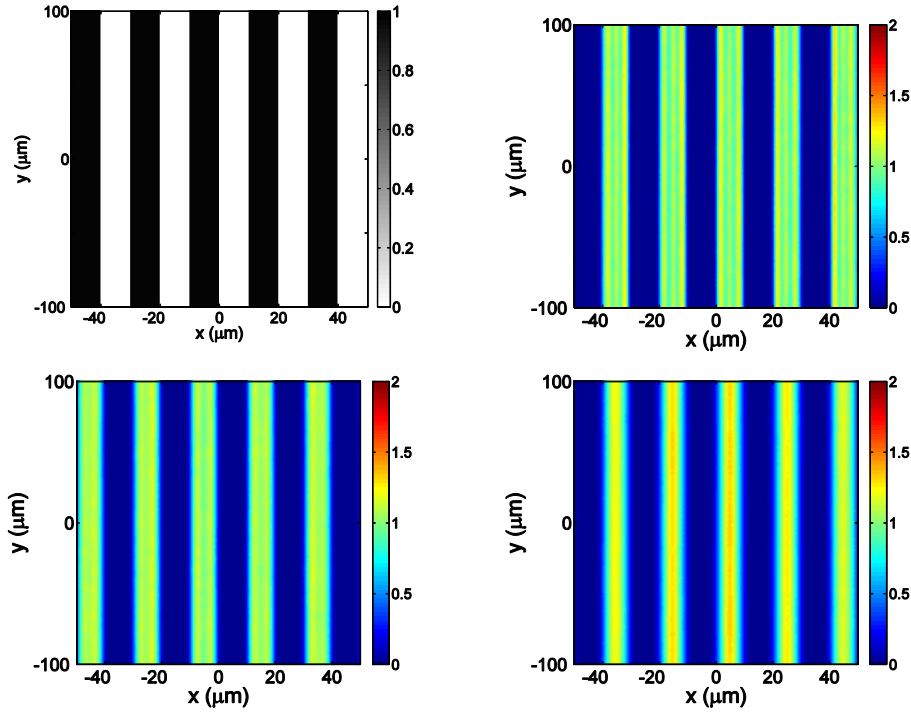
Fig. 3. Perfect grating and first three self-images obtained using the Rayleigh-Sommerfeld approach. The period of the grating is $p = 20$ μm and the wavelength is $\lambda = 0.68$ μm .
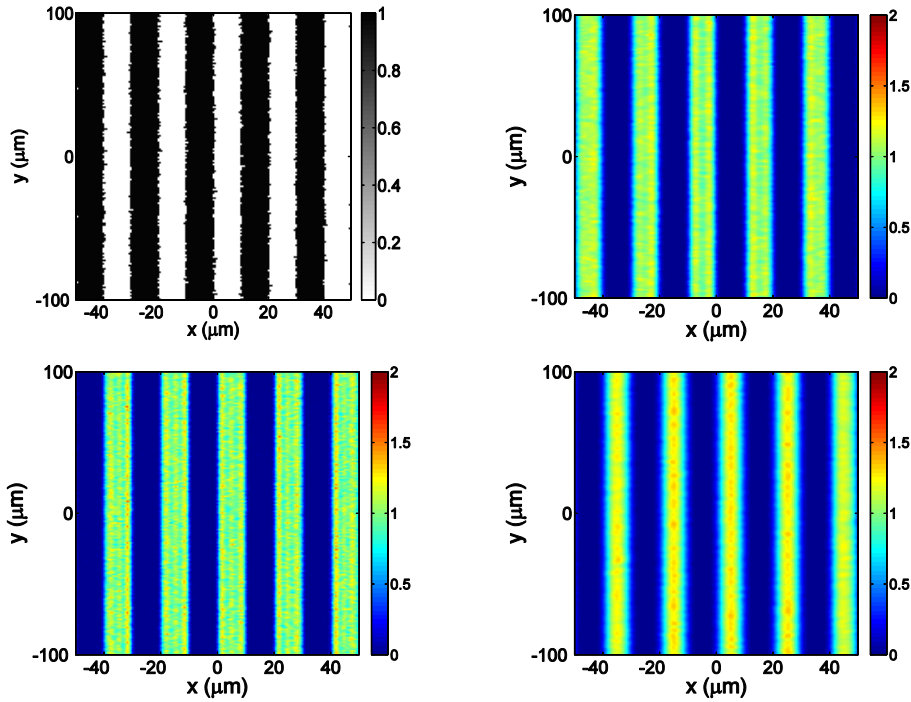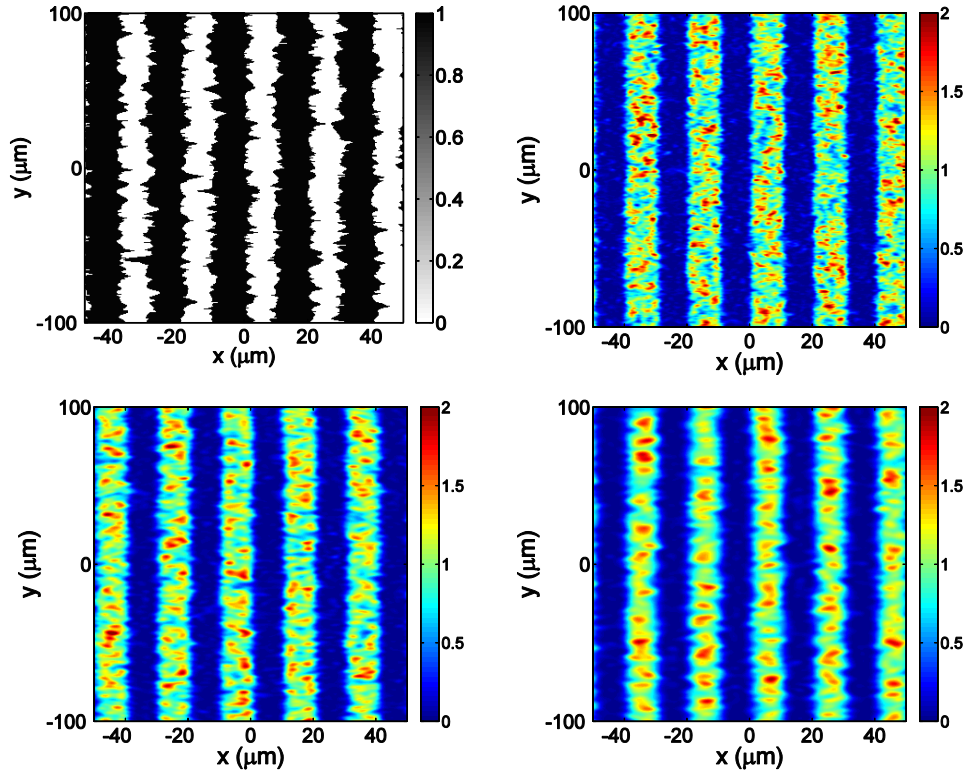

Fig. 4. Grating and first three self-images obtained using the Rayleigh-Sommerfeld approach for the same situation of Fig. 3 when the roughness parameters are $T = 0.1$ μm , $\sigma = .25$ μm .
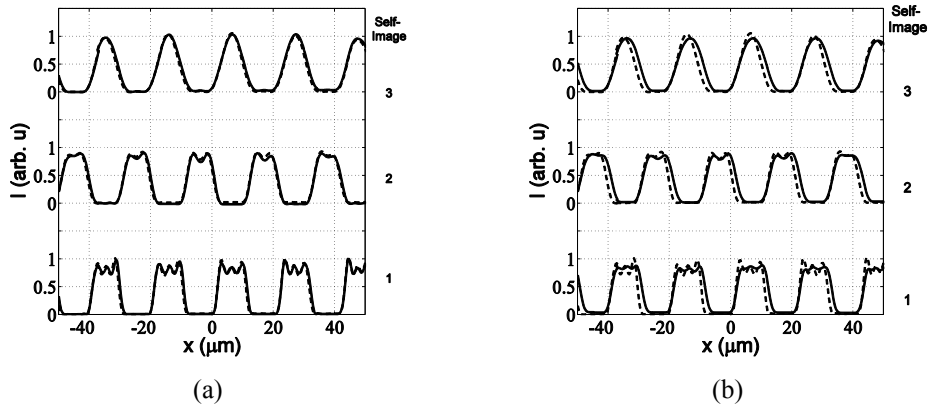
In Fig. 6, a comparison of the average profiles obtained with the perfect grating and the rough gratings is shown. In Fig. 7 (Media 1) a video is included where the transition between $z = 0$ and the first self-image is shown. The intensity distribution at fractional Talbot planes is also shown in Fig. 7 (Media 1) for distances $z = z_T / 4$, $z_T / 3$, $z_T / 2$, and also the average profile for these particular cases.

Fig. 5. Grating and first three self-images obtained using the Rayleigh-Sommerfeld approach for the same situation of Fig. 3 when the roughness parameters are $T = 1\,\mu m$, $\sigma = 1\,\mu m$.

(a)   (b)

Fig. 6. Comparison of the average profiles for the first three self-images for two different roughness levels a) for the parameters of Fig. 4 (b) for the parameters of Fig. 5. Grating with rough edges (solid line), perfect grating, Fig. 3 (dash line).
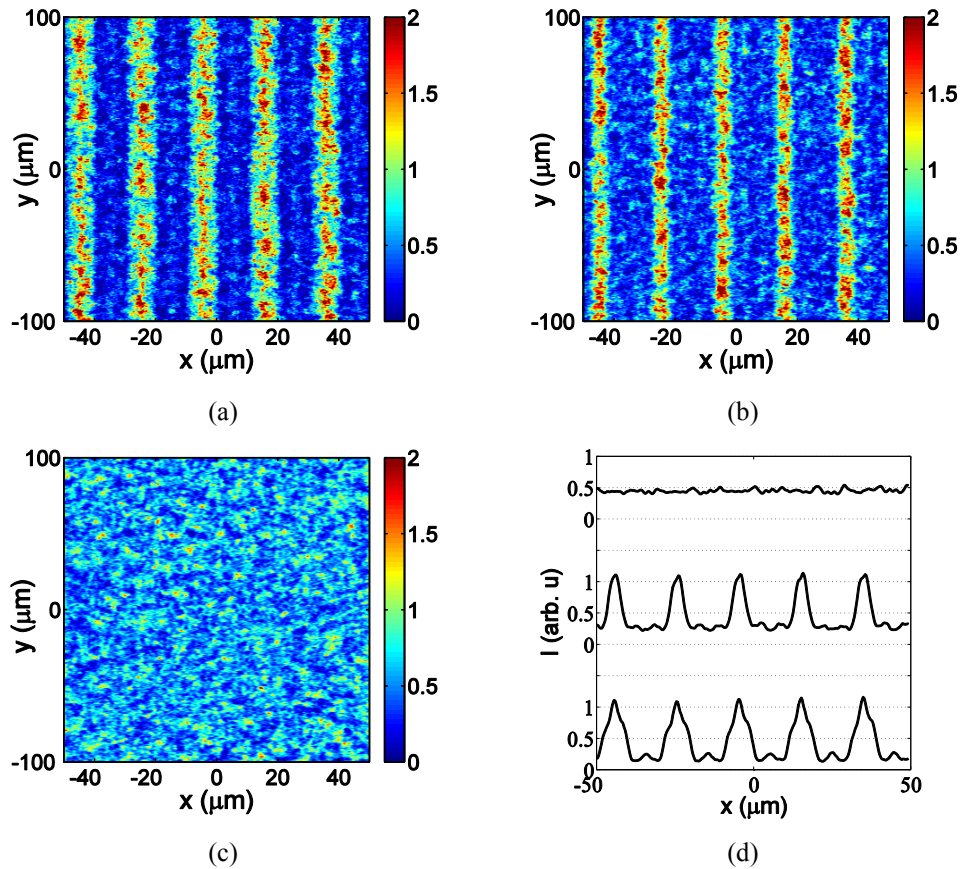
Fig. 7. Fractional self-images for a grating with period $p = 20\,\mu m$, the roughness parameters are $T = 1\,\mu m$ and $\sigma = 1\,\mu m$, and the wavelength is $\lambda = 0.68\,\mu m$ for positions a) $z = z_T / 4$, b) $z = z_T / 3$, c) $z = z_T / 2$ and d) average profiles for this fractional self-images. (Media 1).

3.1. Average intensity distribution

The grating can be placed in a mobile device and then the intensity pattern will be an average over a group of discrete intensity patterns. To characterize this, we calculate the near field intensity pattern for several realizations and then we perform an averaging in the intensity of these realizations. This procedure is repeated for different self images placed at $z = np^2 / \lambda$, with $n = 1, 2, \dots$. The average intensity of these self-images is shown in Fig. 8 for an ensemble of 100 images. For this case, the self-images are very smooth.

4. Experimental approach

To confirm the validity of the results and to use a grating with roughness parameters known, we have manufactured a grating with rough edges using a direct laser photoplotter. The grating is an amplitude grating made of chrome on glass and its period is $p = 100\,\mu m$. The grating is illuminated with a collimated laser diode whose wavelength is $\lambda = 0.65\,\mu m$. In the near field approximation, some self-images have been acquired. For this, we have used a CMOS camera (ueye, pixel size: 6x6 microns) and a microscope objective in order to get a better resolution. In Fig. 9 (Media 2) we can observe the image of the grating using an optical

microscope and the first three self-images taken with the CMOS camera. These images correspond to just one realization. As it can be seen, experimental results are in total accordance with the numerical results. The shape of the self-images is quite smooth compared to the shape of the strips edges. In the self-images we can also see a defect in one of the strips (rectangle) which gradually disappears as the order of the self-image increases. In Fig. 9 (Media 2) a video with the experimental images is also shown.
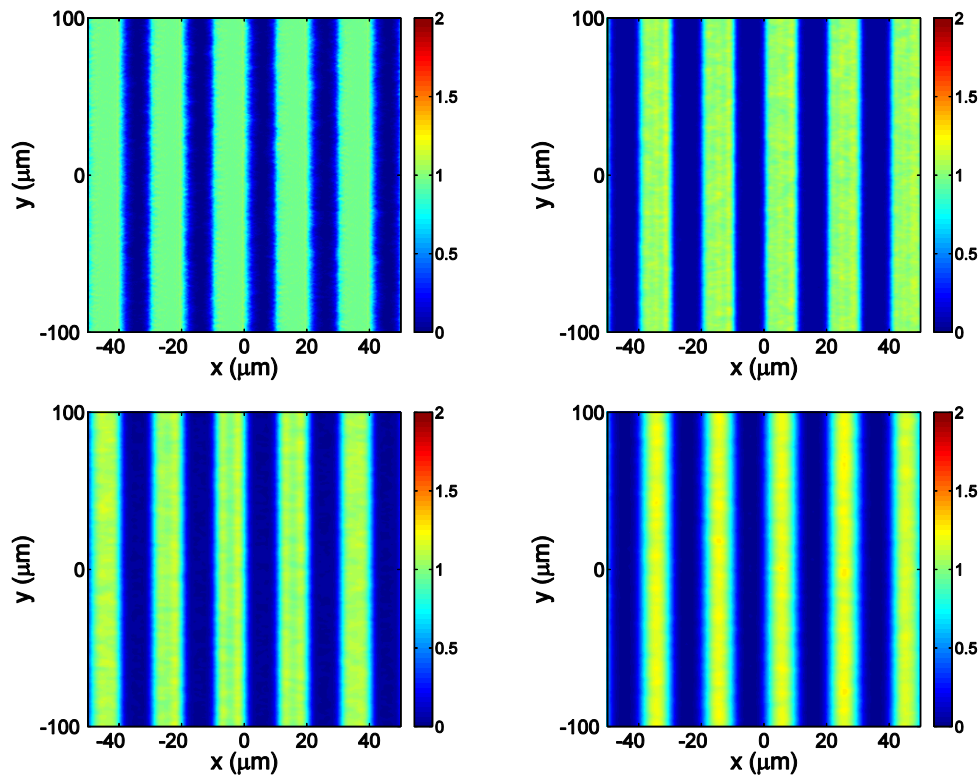
Fig. 8. Average for the first four self-images obtained using the Rayleigh-Sommerfeld approach. The number of samples was 100, the period of the grating is $p = 20\ \mu m$ and the roughness parameters are $T = 1\ \mu m$ and $\sigma = 1\ \mu m$. The wavelength of the incident beam is $\lambda = 0.65\ \mu m$.

The mean profile of these self-images is also shown in Fig. 10 and also the intensity distribution of self-image 15. The intensity at $x = 200 \mu m$ distribution is very smooth except for a dust particle in the optics that we could not eliminate. Comparing this result with that shown in Fig. 6, we can validate the results given by the numerical analysis.
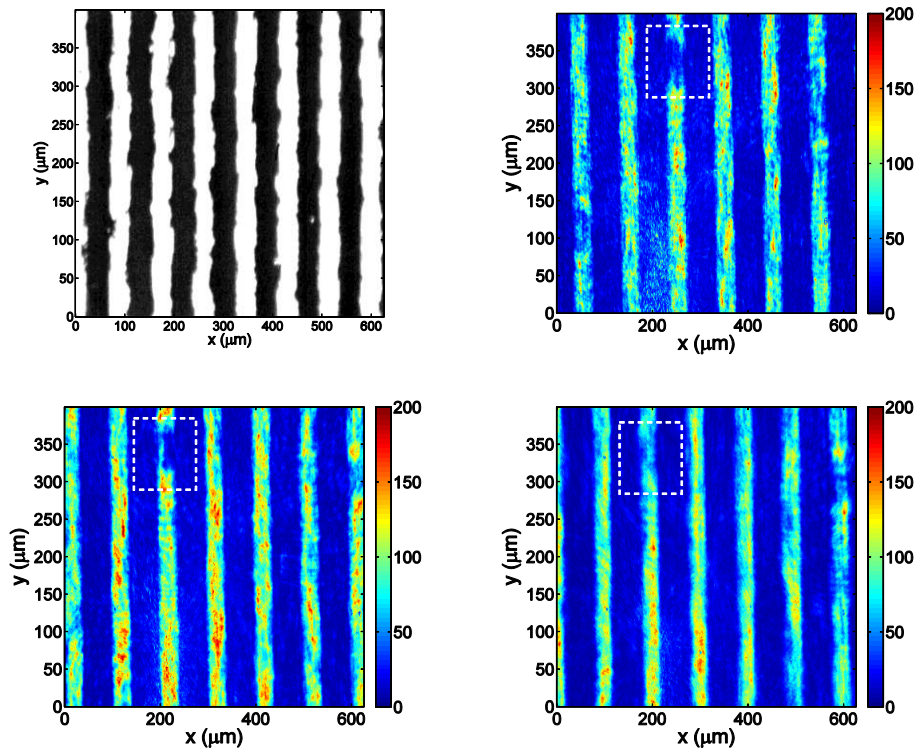
Fig. 9. Optical image of the manufactured diffraction grating with rough edges and experimental first three self-images. The period of the grating is $p = 100\ \mu m$, the wavelength is $\lambda = 0.65\ \mu m$. The roughness parameters used are $T = 50\ \mu m$ and $\sigma = 5\ \mu m$ The images are captured with a CMOS camera whose pixel size is $6\ \mu m \times 6\ \mu m$ and a $30\times$ microscope objective. (Media 2).

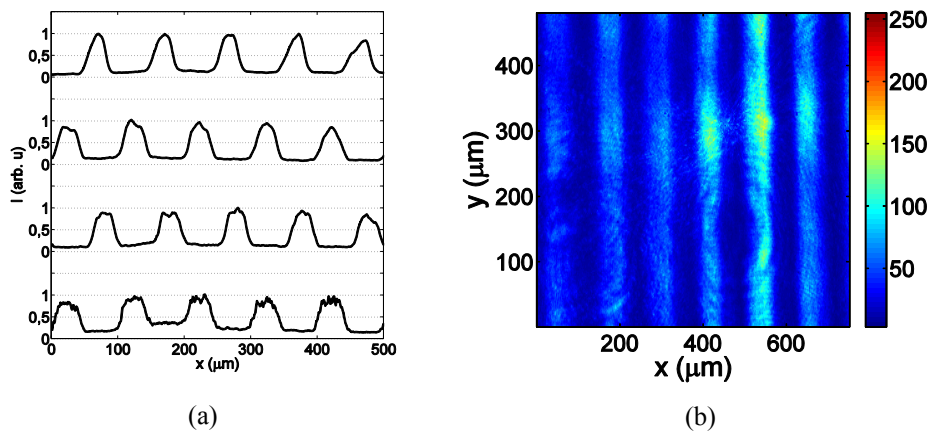(a)   (b)

Fig. 10 (a) Mean profile of the image and self-images shown in Fig. 9 (Media 2) and (b) experimental self image for $n = 15$. The intensity distribution is very smooth. The fluctuations at $x = 500\ \mu m$ are due to a dust particle in the optics that we could not eliminate.

5. Conclusions

In this work, we have analyzed the far field and near field diffraction pattern produced by an amplitude grating whose strips present rough edges. Due to the stochastic nature of the grating a statistical approach is performed. In the far field, the intensity of the diffraction orders strongly decreases in terms of the roughness and the index of the diffraction order. Then, a possible application of this kind of gratings is to obtain amplitude binary gratings with only diffraction orders -1, 0 and +1. For the case of near field, an analytical result is not possible and numerical simulations based on a Rayleigh-Sommerfeld approach have been performed. The self-images are smoother than the grating, since Talbot effect is a cooperative effect. Finally, we have fabricated gratings with rough edges and an experimental verification of the theoretical and numerical results is performed.